Correction

NEUROSCIENCE

Correction for "Dominant hemisphere lateralization of cortical parasympathetic control as revealed by frontotemporal dementia," by Christine C. Guo, Virginia E. Sturm, Juan Zhou, Efstathios D. Gennatas, Andrew J. Trujillo, Alice Y. Hua, Richard Crawford, Lara Stables, Joel H. Kramer, Katherine Rankin, Robert W. Levenson, Howard J. Rosen, Bruce L. Miller, and William W. Seeley, which appeared in issue 17, April 26, 2016, of *Proc Natl Acad Sci USA* (113:E2430–E2439; first published April 11, 2016; 10.1073/pnas.1509184113).

The authors note that on page E2430, right column, first paragraph, line 6, "Seeley et al. (17)" should instead appear as "Seeley et al. (17) and see a review by Menon and Uddin (92)."

The authors note that Table 1 appeared incorrectly, with a misplaced reference next to the "bvFTD" column heading. The corrected table appears below.

Table 1. Demographics of main cohort

	HC		bvFTD		Differences
	Mean (SD)	*N*	Mean (SD)	*N*	*t* or χ^2, *P*
Age, y	59.5 (12.2)	19	59.1 (7.3)	17	0.11, 0.91
Gender (M:F)	9:10		12:5		2.00, 0.16*
Handedness (R:L)	17:2		16:1		0.25, 0.62*
Education, y	16.9 (1.9)	19	16.0 (3.0)	17	1.10, 0.28
BMI	25.8 (4.46)	13	28.7 (2.41)	13	−2.08, 0.05
Mean IBI, ms	965.8 (127.0)	19	916.3 (124.6)	17	1.18, 0.25
CVI	4.5 (0.3)	19	4.2 (0.3)	17	3.00, 0.005
RSA	5.8 (0.9)	19	5.1 (0.7)	17	2.58, 0.014
LogHRV	7.6 (0.6)	19	6.8 (0.6)	17	3.63, 0.001
CSI	1.8 (0.7)	19	1.5 (0.7)	17	1.21, 0.23
SCL, μmho	10.4 (7.5)	18	9.0 (6.5)	17	0.83, 0.41
CDR, total	0.0 (0.0)	18	1.4 (0.7)	17	−8.16, < 0.001
CDR, sum of boxes	0.0 (0.0)	18	7.7 (3.7)	17	−8.67, < 0.001
Head translation, mm	0.28 (0.15)	19	0.34 (0.14)	14	1.21, 0.23
Head rotation, °	0.09 (0.04)	18	0.13 (0.06)	14	−1.91, 0.06

*χ^2 test.

www.pnas.org/cgi/doi/10.1073/pnas.1608056113

Dominant hemisphere lateralization of cortical parasympathetic control as revealed by frontotemporal dementia

Christine C. Guo (郭聪)[a,b,c], Virginia E. Sturm[a,b], Juan Zhou[a,b,d], Efstathios D. Gennatas[a,b,e], Andrew J. Trujillo[a,b], Alice Y. Hua[a,b], Richard Crawford[a,b], Lara Stables[a,b], Joel H. Kramer[a,b], Katherine Rankin[a,b], Robert W. Levenson[f], Howard J. Rosen[a,b], Bruce L. Miller[a,b], and William W. Seeley[a,b,g,1]

[a]Memory and Aging Center, University of California, San Francisco, CA 94143-1207; [b]Department of Neurology, University of California, San Francisco, CA 94143; [c]Mental Health Program, Queensland Institute of Medical Research (QIMR) Berghofer, Herston, QLD 4029, Australia; [d]Center for Cognitive Neuroscience, Neuroscience and Behavioral Disorders Program, Duke-National University of Singapore Graduate Medical School, Singapore; [e]Brain and Behavior Laboratory, Department of Psychiatry, University of Pennsylvania, Philadelphia, PA 19104; [f]Department of Psychology, University of California, Berkeley, CA 94720-1650; and [g]Department of Pathology, University of California, San Francisco, CA 94143

Edited by Marcus E. Raichle, Washington University in St. Louis, St. Louis, MO, and approved March 10, 2016 (received for review May 12, 2015)

The brain continuously influences and perceives the physiological condition of the body. Related cortical representations have been proposed to shape emotional experience and guide behavior. Although previous studies have identified brain regions recruited during autonomic processing, neurological lesion studies have yet to delineate the regions critical for maintaining autonomic outflow. Even greater controversy surrounds hemispheric lateralization along the parasympathetic–sympathetic axis. The behavioral variant of frontotemporal dementia (bvFTD), featuring progressive and often asymmetric degeneration that includes the frontoinsular and cingulate cortices, provides a unique lesion model for elucidating brain structures that control autonomic tone. Here, we show that bvFTD is associated with reduced baseline cardiac vagal tone and that this reduction correlates with left-lateralized functional and structural frontoinsular and cingulate cortex deficits and with reduced agreeableness. Our results suggest that networked brain regions in the dominant hemisphere are critical for maintaining an adaptive level of baseline parasympathetic outflow.

emotion | autonomic neuroscience | frontotemporal dementia | salience network | lateralization

The brain controls peripheral autonomic physiology by perceiving the ambient condition of the body and continuously adjusting autonomic tone to maintain homeostasis (1–3). Theorists have long postulated that physiological body states provide a foundation for emotion and feeling (3–7). Bodily states also shape perception and motivate behavior. The appeal of cold water on a hot summer day or the aversion to socializing when feeling sick demonstrate the intimate link between homeostatic regulation and emotional–motivational processing (2). The autonomic nervous system exerts direct control over bodily states via its two major branches: the sympathetic system, associated with energy mobilization, and the parasympathetic system, whose peripheral efferent signals are conveyed chiefly via the vagus nerve and are associated with energy conservation at the whole organism level (8). Perturbations in one or both of these systems are associated with homeostatic instability and diverse pathological feeling states (1, 9–14). Therefore, elucidating the neural mechanisms of autonomic integration represents an important biomedical research priority.

Although the peripheral and brainstem organization of the autonomic nervous system has been well-characterized, especially in nonhuman laboratory mammals (8), how the human cerebral cortex represents and influences the internal milieu remains less clear (4). Task-activation functional MRI (fMRI) and neurological lesion studies suggest that anterior peri-allocortical transition cortices, especially the frontoinsula (FI) (also referred to as ventral anterior insula) and anterior cingulate cortices (ACCs) and midcingulate cortices (MCCs), constitute the cortical autonomic control centers [see reviews by Craig (3), Critchley (4), Thayer et al. (15), and Seeley et al. (16)]. These regions share a close structural and functional relationship and anchor a large-scale intrinsic connectivity network referred to in the neuroimaging literature as the salience network [Seeley et al. (17)]. Although the ACC and FI coactivate in response to diverse emotionally significant stimuli (4, 18), the FI is regarded as an interoceptive sensory association cortex representing afferent information and the ACC as the visceromotor structure that drives autonomic efference (3, 16, 18–20). Some authors have proposed that left-sided (dominant hemisphere) forebrain structures, such as the ACC and anterior insula (aIns), are predominantly involved with maintaining parasympathetic tone whereas homotopic right (nondominant) forebrain regions control sympathetic tone and responses (21–23).

Although appealing, the lateralization model of autonomic control remains controversial (24). Some uncertainty reflects the challenge of detecting lateralized fMRI activations within a system characterized by opponent organization (coordinated and balanced coactivation of physiologically complementary modules). Lesion studies have suffered from small sample sizes and issues relating to whether the lesion produced loss of function or pathophysiological excitation of the affected tissue, producing inconsistent findings across studies (14, 24, 25).

To overcome these challenges, we studied cortical autonomic control in patients with behavioral variant frontotemporal dementia (bvFTD) using a lesion-based structural and functional imaging approach. BvFTD is characterized by a progressive deterioration

Significance

Brain–body interactions are fundamental to physical and mental health. Here, we used a unique brain lesion model to elucidate the neural localization and lateralization of cerebro-cardiac control. Our data revealed that the salience network, an intrinsic connectivity network anchored by the anterior insula and cingulate, is crucial for maintaining basal parasympathetic outflow. Specifically, dominant hemisphere-predominant salience network damage undermined parasympathetic control of the heart. The findings suggest that balanced functional integrity of both hemispheres is vital to maintaining bodily homeostasis.

Author contributions: V.E.S., J.Z., J.H.K., K.R., R.W.L., H.J.R., B.L.M., and W.W.S. designed research; C.C.G., J.Z., E.D.G., A.J.T., A.Y.H., R.C., and L.S. performed research; C.C.G. contributed new reagents/analytic tools; C.C.G., V.E.S., and A.J.T. analyzed data; and C.C.G., V.E.S., R.W.L., and W.W.S. wrote the paper.

The authors declare no conflict of interest.

This article is a PNAS Direct Submission.

[1]To whom correspondence should be addressed. Email: wseeley@memory.ucsf.edu.

This article contains supporting information online at www.pnas.org/lookup/suppl/doi:10.1073/pnas.1509184113/-/DCSupplemental.

www.pnas.org/cgi/doi/10.1073/pnas.1509184113

of social–emotional functions and diminished phasic autonomic responses during social–emotional tasks (26, 27). Anatomically, bvFTD involves degeneration of core salience network structures proposed to support autonomic regulation, including the ACC and anterior midcingulate cortex (aMCC), FI, and subcortical, limbic, and brainstem sites (28, 29). With graded, often asymmetric damage localized to the relevant network, bvFTD provides an important yet unexplored lesion model for clarifying the neuroanatomy of autonomic control.

Here, we show that patients with bvFTD exhibit diminished basal cardiac vagal tone. Four convergent task-free fMRI analyses revealed that lower cardiac vagal tone was associated with perturbed connectivity in the pregenual and subgenual ACC and FI, predominantly on the left side. Consistent with this leftward functional lateralization, more severe atrophy within the left than right ACC and FI predicted lower cardiac vagal tone and lower agreeableness, an emotional trait that has been associated with vagal tone and fosters social relationships by promoting concern for others (30–33). These findings provide compelling evidence that human cortical parasympathetic control is critically dependent upon a left-lateralized network anchored by the ACC and FI.

Results

Seventeen patients with bvFTD and 19 healthy controls (HCs), all taking no relevant medications, underwent task-free fMRI while their peripheral autonomic physiological signals were recorded (*Methods*). We examined baseline ("resting") autonomic activity and the structural and functional imaging correlates of that activity.

The heart is thought to function under continuous regulation by a central autonomic network made up of the ACC, aIns, amygdala, hypothalamus, periaqueductal gray, and other brainstem integration centers (34). The efferent projections of this network are thought to maintain cardiac vagal tone. Under baseline or "resting" conditions, like those studied here, heart rate is determined by vagal suppression of the sinoatrial node pacemaker, such that the normal resting heart rate of 60–80 beats per minute falls well below the "intrinsic" rate of 100–110 beats per minute. Small, rapid adjustments in vagal heart rate suppression, such as those that accompany respiration, give rise to normal heart rate variability. Based on these considerations and the availability of high quality in-scanner heart rate data, we focused our analyses on cardiac vagal tone.

bvFTD Is Associated with Reduced Cardiac Vagal Tone. First, we sought to determine the impact of bvFTD on baseline autonomic physiology. We compared the bvFTD and control groups with regard to their overall cardiac vagal tone, as measured by the cardiac vagal index (CVI), the logarithm of the heart rate variability (logHRV) and respiratory sinus arrhythmia (RSA), as measured by the high frequency power of cardiac activity (35), over an 8-min (eyes closed) task-free fMRI session. As expected, CVI, logHRV, and RSA were highly correlated (Pearson's $r > 0.87$), and we used all three measures in group comparisons for additional validation. Overall cardiac vagal tone was significantly lower in bvFTD, suggesting that bvFTD is associated with diminished parasympathetic tone at rest (Fig. 1*A* and Table 1) [$P = 0.005$ (CVI), $P = 0.001$ (logHRV), and $P = 0.014$ (RSA), two-sample t test]. Consistent with diminished parasympathetic influence, patients with bvFTD showed higher resting heart rate than healthy controls although this difference did not reach statistical significance (Fig. 1*B* and Table 1) ($P = 0.25$, two-sample t test). Skin conductance level (SCL), a marker for sympathetic outflow, showed no difference between groups (Fig. 1*C* and Table 1) ($P = 0.41$, two-sample t test). Another common measure of sympathetic activity, the frequency of spontaneous skin conductance responses, did not differ between bvFTD and controls ($P = 0.12$, two-sample t test). The reduction of cardiac vagal tone in bvFTD was unlikely due to confounding factors including age, gender, body mass index (BMI), or handedness because the effects persisted after controlling for these variables in a general linear model (GLM) analysis (*SI Appendix*, Table S1) [$P = 0.03$ (CVI), $P = 0.02$ (logHRV), and $P = 0.04$ (RSA), GLM]. To further exclude possible gender effects, we confirmed the bvFTD-associated cardiac vagal tone deficits in smaller but age- and gender-balanced groups (*SI Appendix*, Table S2) [$P = 0.012$ (CVI), $P = 0.003$ (logHRV), and $P = 0.015$ (RSA), two-sample t test].

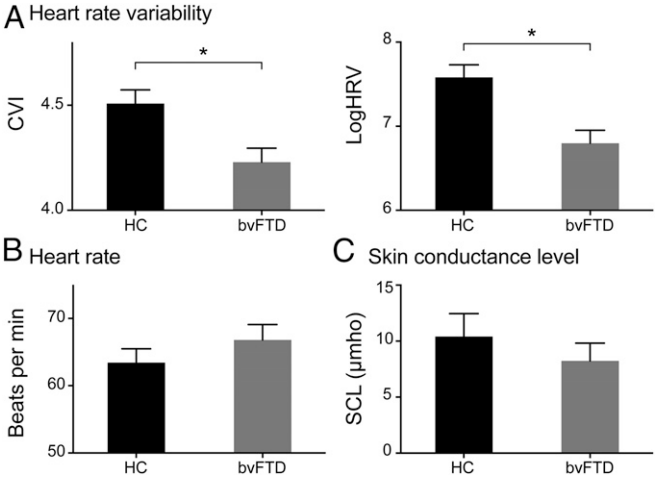

Fig. 1. Autonomic activity at rest in HC and bvFTD. (*A*) Heart rate variability, as measured by CVI (*Left*) and logHRV (*Right*), (*B*) heart rate, as measured by mean IBI, and (*C*) skin conductance level in HC and bvFTD groups. Error bars signify SE mean. An * signifies significant differences ($P < 0.05$) between HC and bvFTD.

To determine whether the bvFTD-related reduction in cardiac vagal tone reflects a nonspecific effect of neurodegeneration, we expanded the comparison to include eight age-matched patients with Alzheimer's disease (AD) for whom linked imaging and autonomic data were available. Cardiac vagal tone showed significant group differences (*SI Appendix*, Fig. S1 and Table S3) [$P = 0.003$ (CVI), $P < 0.001$ (logHRV), and $P = 0.006$ (RSA), ANOVA], driven by the significantly lower values in bvFTD compared with AD and HC [$P < 0.015$ (CVI), $P < 0.002$ (logHRV), and $P < 0.01$ (RSA), post hoc Tukey tests], with no significant differences between AD and HC [$P = 0.84$ (CVI), $P = 0.72$ (logHRV), and $P = 0.76$ (RSA), post hoc Tukey tests]. The significant group differences in cardiac vagal tone were not explained by confounding factors including age, gender, medication (donepezil), or handedness (*SI Appendix*, Table S4) [$P = 0.004$ (CVI), $P = 0.002$ (logHRV), and $P = 0.003$ (RSA), GLM].

Left-Lateralized Disruption of Brain–Heart Coupling in bvFTD. Considering the diminished cardiac vagal tone in bvFTD and the impact of this disorder on cortical autonomic control sites, we hypothesized that bvFTD would disrupt coupling between heart rate variability and activity in cortical regions involved in efferent and afferent cortical autonomic representations. To test this hypothesis, we derived a moment-to-moment continuous heart rate variability (HRV) index by moving an 18-second sliding window across each 8-min fMRI session, producing 240 HRV data points [one aligned to each repetition time (TR)] (*SI Appendix*, Fig. S2) (*Methods*). The validity of this continuous HRV index was supported by correlating its average over the entire 8-min session with overall cardiac vagal tone as indexed by the CVI (*SI Appendix*, Fig. S2) ($r = 0.97$, $P < 0.0001$, Pearson correlation). Only right-handed subjects were included in the following analyses.

In healthy controls, continuous HRV correlated directly with blood oxygen level-dependent (BOLD) signal in the aMCC,

Table 1. Demographics of main cohort

	HC		bvFTD (92)		Differences
	Mean (SD)	*N*	Mean (SD)	*N*	*t* or χ^2, *P*
Age, y	59.5 (12.2)	19	59.1 (7.3)	17	0.11, 0.91
Gender, M:F	9:10		12:5		2.00, 0.16*
Handedness, R:L	17:2		16:1		0.25, 0.62*
Education, y	16.9 (1.9)	19	16.0 (3.0)	17	1.10, 0.28
BMI	25.8 (4.46)	13	28.7 (2.41)	13	−2.08, 0.05
Mean IBI, ms	965.8 (127.0)	19	916.3 (124.6)	17	1.18, 0.25
CVI	4.5 (0.3)	19	4.2 (0.3)	17	3.00, 0.005
RSA	5.8 (0.9)	19	5.1 (0.7)	17	2.58, 0.014
LogHRV	7.6 (0.6)	19	6.8 (0.6)	17	3.63, 0.001
CSI	1.8 (0.7)	19	1.5 (0.7)	17	1.21, 0.23
SCL, μmho	10.4 (7.5)	18	9.0 (6.5)	17	0.83, 0.41
CDR, total	0.0 (0.0)	18	1.4 (0.7)	17	−8.16, <0.001
CDR, sum of boxes	0.0 (0.0)	18	7.7 (3.7)	17	−8.67, <0.001
Head translation, mm	0.28 (0.15)	19	0.34 (0.14)	14	1.21, 0.23
Head rotation, °	0.09 (0.04)	18	0.13 (0.06)	14	−1.91, 0.06

*χ^2 test.

predominantly on the left, and the left aIns (Fig. 2*A*) [$P < 0.001$ for height and false discovery rate (FDR)-corrected $P < 0.05$ for cluster extent] (see *SI Appendix*, Table S5 for coordinates). At a more liberal threshold, the pregenual ACC, right aIns, and inferior frontal gyrus (IFG) were also coupled with HRV (Fig. 2*A*) ($P < 0.005$ for height and FDR-corrected $P < 0.05$ for cluster extent) (see *SI Appendix*, Table S5 for coordinates). These healthy control findings, broadly consistent with the literature (15), confirmed the validity of our approach and enabled a comparison of brain–heart coupling between bvFTD and HC.

Coupling between HRV and BOLD signal was reduced in bvFTD compared with controls in the subgenual ACC and left FI (Fig. 2*B*) (*SI Appendix*, Table S5) ($P < 0.01$ for height and $P < 0.05$ for cluster extent). This reduction was unlikely due to the impaired baseline cardiac vagal tone in patients, i.e., floor effects, because including overall CVI as a nuisance covariate did not change the results. Additionally, these results remained significant after voxel-wise gray matter intensity maps were included as covariates. No regions showed greater heart–brain coupling in bvFTD than in controls. These findings could represent bvFTD-associated impairments in cortical efferent cardiac control or failures to continuously rerepresent vagal feedback from the heart within the cortex or both.

Salience Network Connectivity Correlates with Overall HRV. BvFTD is a network-based disorder in which atrophy and diminished intrinsic connectivity emerge within the bilateral ACC, FI, and the "salience network" anchored by these key cortical hubs (28, 36–38). We therefore sought to determine whether cardiac vagal tone correlates not only with the moment-to-moment activity of these regions (Fig. 2) but also with their intrinsic connectivity during task-free conditions, a metric with moderate trait stability (39) that predicts intersubject variability of emotional experience and social behavior (17, 40). Here, we present correlation analyses between CVI and intrinsic connectivity across patient and control groups (Fig. 3) because analysis with logHRV and RSA yielded similar results.

First, we used a seed-based approach to examine the relationship between CVI and salience network connectivity. Following previous studies (29, 39), we used a seed in the right FI to derive the salience network, as well as a mirror image left FI seed to evaluate laterality effects. Right FI connectivity was related to CVI but predominantly through its interactions with left-sided structures, including FI, the inferior frontal gyrus, and the anterior temporal lobe (Fig. 3*A*) [$P < 0.001$ (red) or 0.005 (yellow) for height and FDR-corrected $P < 0.05$ for cluster extent] (see *SI Appendix*, Table S5 for coordinates). Left FI connectivity strengths predicting CVI, in contrast, were predominantly ipsilateral and included the adjacent left aIns, subgenual ACC, temporal pole, occipital lobe, and ventral putamen (Fig. 3*B*) (see *SI Appendix*, Table S5 for coordinates). To ensure sufficient statistical power for the whole brain significance tests, these correlation analyses were performed across patients and controls, with group included as a covariate. The correlation between the most significant clusters, including the left aIns and subgenual ACC, and CVI remained significant when tested separately in bvFTD and HC (*SI Appendix*, Fig. S3) ($P < 0.05$, post hoc Pearson correlation), with no significant differences in the slopes between the two groups ($P > 0.1$, ANCOVA).

The seed-based intrinsic connectivity analyses described above are inherently biased by seed selection. To seek convergent support while avoiding regional bias, we turned to whole brain graph theoretical analysis, a seed-independent approach that quantifies the connectedness of each node in the whole brain

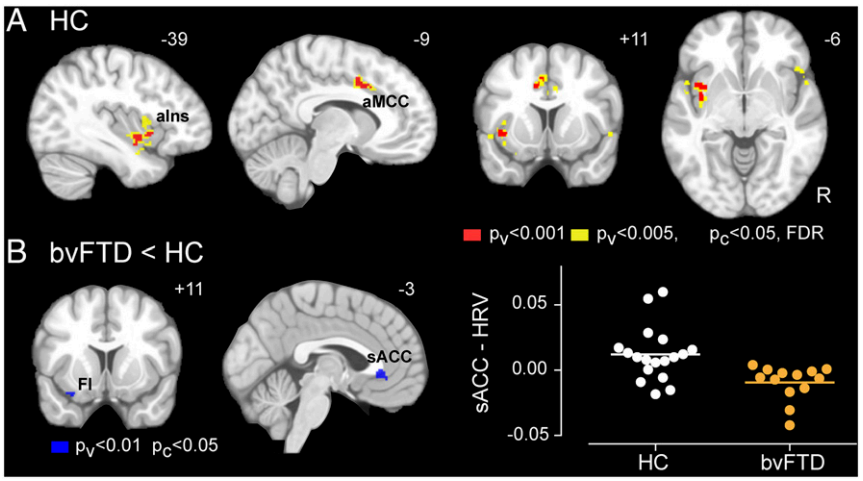

Fig. 2. Heart–brain coupling. (*A*) Coupling between BOLD activity and continuous HRV in HC, generated with a joint height-extent threshold [$P < 0.001$ (red) or 0.005 (yellow) for peak height and FDR-corrected $P < 0.05$ for spatial extent]. (*B*) Group differences (bvFTD < HC) in HRV-BOLD coupling, generated with a joint height-extent threshold ($P < 0.01$ for peak height and $P < 0.05$ for spatial extent). Data from the cluster in the subgenual anterior cingulate cortex (sACC) are plotted on the *Right*. aIns, anterior insula; aMCC, anterior midcingulate cortex; FI, frontoinsula.

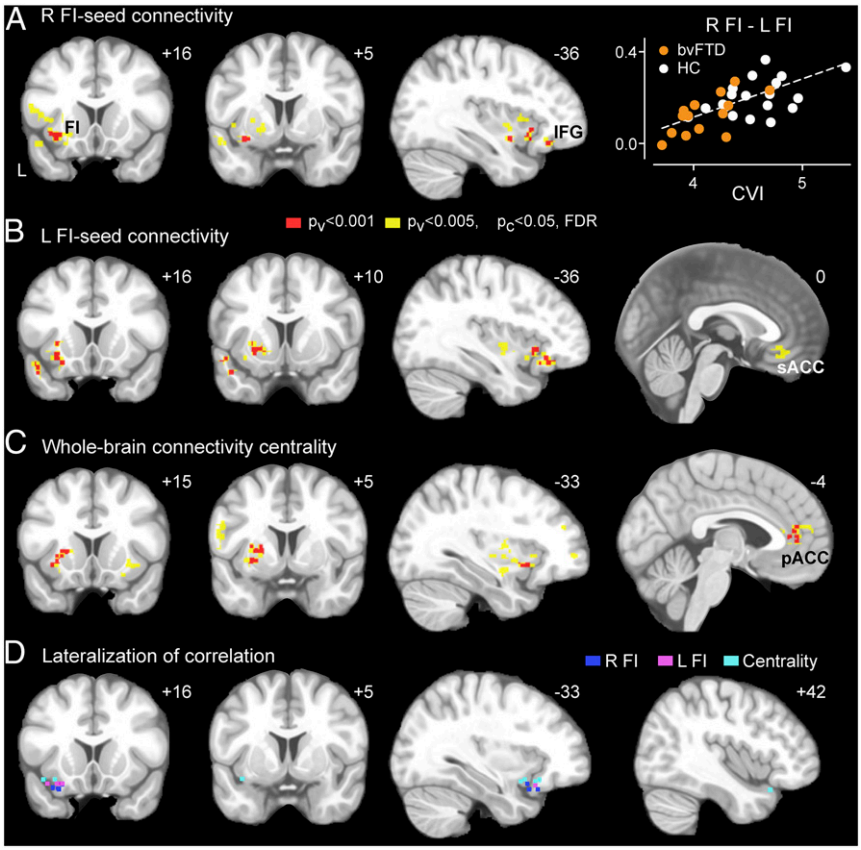

Fig. 3. Correlation between intrinsic connectivity and cardiac vagal tone. (*A*) Right FI-seeded, (*B*) left FI-seeded, and (*C*) whole-brain intrinsic connectivity maps were correlated with CVI in HC and bvFTD groups. Results were generated with a joint height-extent threshold [$P < 0.001$ (red) or 0.005 (yellow) for peak height and FDR-corrected $P < 0.01$ for spatial extent]. (*A*) Data from the cluster in the left FI are plotted on the right panel. (*D*) Voxels with significant lateralization effect in their correlations with CVI. Voxels are shown in the left hemisphere if their correlations with CVI are significantly stronger on the left than the right or in the right hemisphere if their correlations with CVI are significantly stronger on the right than the left ($P < 0.05$). Results from the three functional connectivity maps are overlaid on the same template brain. FI, frontoinsula; IFG, inferior frontal gyrus; pACC, pregenual anterior cingulate cortex; sACC, subgenual anterior cingulate cortex.

network. Although the optimal method for defining network nodes and their connectivity remains an area of active research, here we opted for an unbiased and high resolution voxel-wise method in which the connectedness of each voxel is defined as its weighted degree centrality within the whole brain network (*Methods*) (41). This analysis converged with the seed-based analyses, revealing that connectivity degree centrality of the pregenual ACC and left FI significantly correlated with cardiac vagal tone (Fig. 3*C*) [$P < 0.001$ (red) or 0.005 (yellow) for height and FDR-corrected $P < 0.05$ for cluster extent] (see *SI Appendix*, Table S5 for coordinates); this correlation remained significant when tested separately in bvFTD and HC (*SI Appendix*, Fig. S3) ($P < 0.05$, post hoc Pearson correlation). Additional clusters were found in the left middle temporal gyrus, left dorsolateral prefrontal cortex, and bilateral putamen and cerebellum. Clusters identified in these correlation analyses remained significant after voxel-wise gray matter intensity maps were included as covariates.

Overall, these task-free fMRI findings suggest that the intrinsic functional connections of the left ACC and FI play a hemispherically dominant role in regulating cardiac vagal tone. To confirm this apparent lateralization effect, we performed voxel-wise statistical comparisons between all left and right hemisphere voxels showing even a weak relationship to CVI ($P < 0.01$, uncorrected) (*Methods*). We found that the voxels with significant lateralization effects localize predominantly to the left anterior insula (Steiger's test, $P < 0.05$) (Fig. 3*D*), confirming the lateralization patterns observed visually. No significant lateralization effect was detected in the ACC.

Leftward Asymmetry of bvFTD Atrophy Predicts Reduced Cardiac Vagal Tone. The preceding fMRI analyses support the view that the ACC, FI, and related structures, predominantly on the left, participate in regulating cardiac vagal tone, either by generating or by rerepresenting cardiac parasympathetic signals (21). Patients with bvFTD, however, offer a unique opportunity to determine whether these regions prove critical for maintaining normal cardiac vagal tone. In contrast to traditional lesion deficit-mapping studies, which classify lesions as present or absent in each region, bvFTD provides a graded, quantifiable, and often asymmetric neurodegenerative lesion, as exemplified by the present bvFTD sample (*SI Appendix*, Fig. S4*A*). Here, we quantified the differential atrophy between the left and right sides of the salience network using a lateralization index, for which a score of zero indicates symmetric brain volume, whereas scores less than or greater than zero indicate more severe left- or right-sided atrophy, respectively. This approach revealed that left-worse-than-right atrophy within the salience network was associated with lower basal CVI (Fig. 4*A*) ($r = 0.45$, $P < 0.01$, Pearson correlation). Importantly, the absolute severity of the left-sided atrophy was a poor predictor of CVI (*SI Appendix*, Fig. S4*B*) ($r = -0.16$, $P = 0.50$, Pearson correlation). Thus, only by capturing the graded lateralization of the salience network lesion

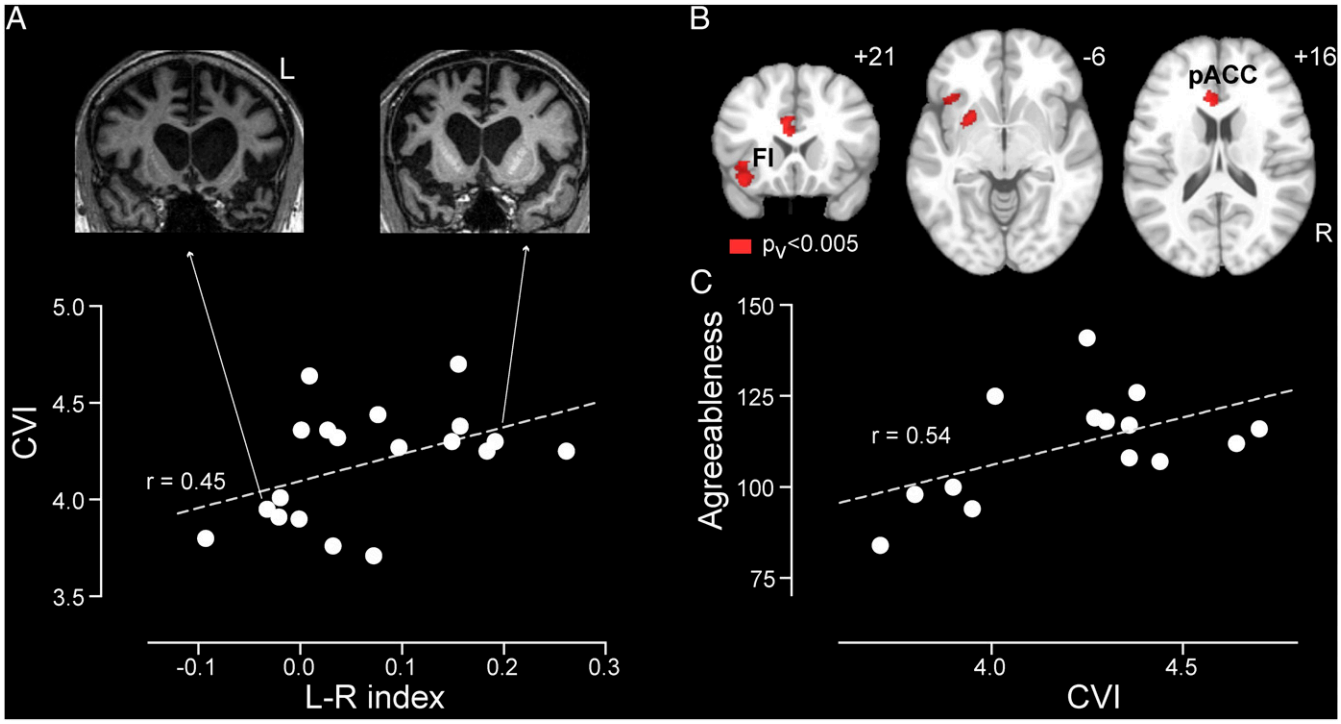

Fig. 4. Correlation analyses of cardiac vagal tone with brain structural asymmetry and positive emotion in bvFTD. (*A*) CVI plotted against left vs. right salience network lateralization index for the bvFTD group. Structural MR images are shown for two representative patients whose brain atrophy was strongly lateralized. (*B*) Correlation analysis between voxel-wise lateralization index and CVI ($P < 0.005$). FI, frontoinsula; pACC, pregenual anterior cingulate cortex. (*C*) Agreeableness plotted against CVI for the bvFTD group.

were we able to uncover the critical role for the left hemisphere in maintaining cardiac vagal tone.

To determine which brain structures within the salience network drive the leftward lateralization of cardiac vagal efference, we developed a voxel-wise lateralization method for quantifying left- vs. right-sided atrophy severity for each voxel (*Methods*). We then performed a correlation analysis with CVI as the independent variable of interest and voxel-wise asymmetry scores as the dependent variables. Remarkably, this analysis revealed that left-worse-than-right atrophy involving the pregenual ACC and FI correlated with lower CVI (Fig. 4*B*) ($P < 0.005$ for height). Right-worse-than-left atrophy, in contrast, showed no correlations with reduced CVI. These observations show that basal cardiac vagal tone depends on a normal balance between left- and right-sided structural integrity within regions that activate during autonomic processing such that asymmetric dominant hemisphere damage predicts greater parasympathetic dysfunction.

Cardiac Vagal Tone Correlates with Trait Agreeableness. Finally, we examined whether impaired cardiac vagal tone was associated with characteristic behavioral deficits in bvFTD, such as loss of interpersonal warmth and interest in the emotional lives of others (33, 42). The parasympathetic nervous system is thought to facilitate social engagement by slowing the heart and fostering a calm state necessary for attunement to others' emotional needs (43). In healthy individuals, higher resting vagal tone has been associated with more frequent feelings of positive emotional experience and social connection (44) as well as with more positive mood, optimism, agreeableness, and extraversion (31). To examine the relationship between parasympathetic deficits and emotion in bvFTD, we selected two questionnaire-based personality measures, the construct "agreeableness" and the facet "positive emotion" from the Neuroticism-Extraversion-Openness Personality Inventory-3 (NEO-PI-3) (32). We found that lower cardiac vagal tone, assessed by either CVI (Fig. 4*C*) ($r = 0.54$, $P = 0.019$, Pearson correlation) or logHRV ($r = 0.42$, $P = 0.023$), was associated with diminished agreeableness, even after controlling for age, gender, and BMI. The correlation between cardiac vagal tone and positive emotion, the tendency to experience positive emotions such as happiness, was in the same direction but not significant ($r = 0.15$, $P = 0.2$, Pearson correlation). We then performed additional exploratory analyses to assess the specificity of these correlations. Cardiac vagal tone was not correlated with the anxiety or depression subscales on NEO-PI-3 ($P > 0.4$, $r < 0.2$), suggesting that our findings cannot be accounted for by nonspecific mood disturbance. We further observed no correlation with Neuropsychiatric Inventory subscales for apathy or disinhibition, two core symptoms of bvFTD ($P > 0.3$, $r < 0.3$).

Further brain–behavioral correlation analysis revealed that agreeableness significantly correlated with the salience network lateralization index ($r = 0.54$, $P = 0.02$, Pearson correlation) such that more left-sided atrophy was associated with lower agreeableness. These results suggest that the salience network, predominantly on the left side, provides an anatomical basis for the relationship between cardiac vagal tone and positive emotion regulation. Finally, because a left-lateralized pattern was observed, we asked whether speech and language problems could have had an indirect impact on agreeableness, due to, for example, the frustration induced by communication difficulties. We assessed this possibility by correlating several speech/language scores with agreeableness and found no correlation, suggesting that the correlation between left salience network atrophy and declining agreeableness is unlikely to be mediated by speech/language difficulties ($P > 0.2$, $r < 0.35$; scores tested include verbal ability, irregular word reading, syntax comprehension, Boston naming test, lexical fluency, and semantic fluency).

Discussion

BvFTD provides a unique lesion model in which graded, often asymmetric damage occurs in structures within the putative cortical autonomic control system. Capitalizing on this opportunity, we found that left hemisphere-predominant anterior insula and cingulate cortex dysfunction and degeneration were associated with impaired baseline parasympathetic outflow, as indexed by cardiac vagal tone. In particular, diminished cardiac vagal tone was associated with reduced (*i*) moment-to-moment heart–brain coupling, (*ii*) left-predominant salience network intrinsic connectivity and structural integrity, and (*iii*) trait agreeableness. Throughout these analyses, the anterior cingulate and insular cortices stood out as the structures whose functional and structural integrity was most critical, making a left hemisphere-predominant contribution to maintaining parasympathetic outflow.

Localization and Lateralization of Cortical Cardiac Parasympathetic Control. It has been argued that cortical autonomic efferent and afferent representations are lateralized in the forebrain, with parasympathetic representations in the dominant hemisphere and sympathetic representations on the nondominant side (21, 23, 45–47). This lateralization framework remains controversial, however, due to inconsistencies in the human lesion literature. Most previous studies have been small or limited by the clinical context or methodology. In five patients undergoing surgery for epilepsy, left insula stimulation produced parasympathetic effects (bradycardia and blood pressure depression) whereas stimulation of the right insula produced sympathetic effects (tachycardia and blood pressure elevation) (23). Conversely, inactivating the left hemisphere with intracarotid amobarbital was associated with increased sympathetic activity and decreased vagal tone in small series (45, 47, 48). Convergent evidence was observed in ischemic lesion studies. Acute left hemisphere stroke was associated with reduced cardiac vagal tone and increased cardiac sympathetic tone (49); similar lateralization was observed in seven patients with focal insular stroke (22). Furthermore, a study in which healthy subjects viewed short films presented to either the left or right visual hemifield suggested that the left hemisphere exerted predominant control of parasympathetic modulation of cardiac activity (50). The left-lateralization of vagal control has been challenged, however, by prominent parasympathetic deficits after right hemispheric stroke or epilepsy (25, 51–53) and inconsistent findings using the intracarotid amobarbital test (54). In addition, a prominent neurovisceral model favors right hemispheric control of cardiac vagal function, based on neuroimaging studies using cognitive and affective tasks (14, 24).

Our results provide convergent and rigorous evidence that cortical parasympathetic control is lateralized to the dominant hemisphere in humans. Critically, the balance between the left and right aINS and ACC damage (Fig. 4) superseded the absolute volume loss on either side (*SI Appendix*, Fig. S4*B*) in predicting reductions in cardiac vagal tone. Why did this finding emerge so clearly in this lesion study compared with previous series? As a neurodegenerative disease, bvFTD targets a specific cortical network known to be involved in cardiac autonomic control. This lesion type provides certain advantages over stroke lesions, which may have destructive (suppressing function) or irritative (stimulating function) consequences in the acute phase and often injure fibers of passage, complicating interpretation. Stimulation studies in patients with epilepsy are performed on brains that have undergone dynamic functional reorganization throughout an extended disease course. Our lesion model permits the test of functional lateralization within relevant brain regions; such anatomical specificity is lacking in previous studies using intracarotid amobarbital tests, which inactivate most of one hemisphere at a time. This methodological difference may help us to understand differences between our finding and previous efforts to lateralize parasympathetic function in humans (45, 47, 48, 54). Furthermore, whereas neurodegenerative lesions can pinpoint and lateralize brain regions critical for a given function, fMRI studies often capture bihemispheric homologous structures that, although recruited during task completion, may or may not be necessary for the task (55). This issue represents an important challenge when studying autonomic control because healthy homeostasis constantly balances sympathetic and parasympathetic tone, and perturbations in sympathetic outflow are rapidly compensated by adjustments in parasympathetic tone and vice versa.

Relationship of Cardiac Vagal Tone to Emotional Behavior. Emotion is fundamentally embodied—the bodily or physiological responses to emotional stimuli form the "blood and guts" of emotional experience (24, 56, 57). In particular, the two-way communication between the brain and heart is considered an integral part of emotional well-being (14, 34, 43, 58). Low resting heart rate variability is associated with poor emotion regulation and executive control and has been found in patients with depression, anxiety disorders, and posttraumatic stress disorder (59–62). Even in healthy subjects, higher resting vagal tone has been associated with positive mood, optimism, and personality traits that promote social engagement (31, 44). Exaggerated resting vagal tone, however, may also be maladaptive and put individuals at risk for dysregulated positive emotion (i.e., mania) or reduced prosociality (63, 64).

Our study provides a network-based anatomical account for the relationship between parasympathetic outflow and positive emotion. Previous bvFTD studies have emphasized the role of right hemisphere degeneration in producing the characteristic clinical features of loss of empathy (65), social disinhibition (66), and overeating (67), perhaps by undermining negative emotions such as embarrassment (68) and visceral feelings such as satiety (67). Simple positive emotions are often preserved, at least at the group level, in heterogeneous bvFTD samples (27, 69). Our study provides the more nuanced view that relative injury to the dominant hemisphere autonomic control structures produces a clinical picture that includes reduced parasympathetic outflow and a more irritable, irascible (i.e., less agreeable) patient. The hemispheric lateralization of specific emotion categories, however, has received some conflicting evidence from functional neuroimaging studies in healthy subjects. Although some findings are in line with left dominance for positive emotion, other studies have reported bilateral activations, and recent meta-analyses do not support a simple model of hemispheric lateralization according to emotional valence (70). The present work adds an important piece of human lesion-based evidence to this active area of investigation.

Relationship of Present Findings to Previous Work on Autonomic Processing in bvFTD. Although bvFTD-related damage to cortical autonomic centers such as the ACC and FI has been well-documented, few studies have directly assessed autonomic functions in these patients (12, 13). A recent study performed clinical autonomic function tests and reported a high prevalence of parasympathetic and sympathetic dysfunction in bvFTD without exploring the anatomical correlates of these deficits (13). In the context of emotion processing, several studies examined physiological reactivity to emotional stimuli and found that patients with bvFTD retained physiological responses to many stimuli (27, 71, 72) but that response amplitudes were diminished to emotional stimuli, such as those designed to elicit self-conscious emotions (71). One study linked blunted phasic embarrassment-related, predominantly sympathetic autonomic responses to atrophy of the right pregenual ACC (68). Interestingly, baseline skin conductance level, a measure of sympathetic tone, was recently found to be reduced in patients with

bvFTD (72), in contrast to the lack of a significant difference in our study (Table 1). Our experimental setting could have been insensitive to sympathetic deficits due to the calming influence of the scanner environment on healthy control subjects or an activating influence of the scanner on patients. Further work is needed to examine baseline autonomic physiology in depth outside the scanner.

Limitations and Future Directions. A technical limitation of our study is the use of photoplethysmography for measuring HRV. ECG is the gold standard for detecting heartbeats and deriving HRV, but scanner-related ECG artifact prevented us from using these data. We used pulse wave peaks as an alternative, but this approach lacks the temporal precision of ECG, and, although pulse rate variability provides an acceptable estimation of HRV at rest in healthy young adults (73), its validity has not been addressed in older or clinical populations. Therefore, our results should be interpreted with this caveat in mind, and future studies are needed to replicate our HRV results outside the scanner using ECG and in the scanner through technical improvements in ECG signal acquisition or processing.

Important, nuanced questions about the cortical control of autonomic outflow remain unanswered. Brain structures controlling sympathetic and parasympathetic arms of the system may differ based on task conditions or the end organs being controlled. Our study focused on baseline cardiac vagal tone and thus offers limited insights into phasic autonomic reactivity or the interaction between parasympathetic and sympathetic systems in response to perturbations. Neuroimaging studies in health have suggested that parasympathetic regulation during active task paradigms is closely associated with the default mode network (74). Therefore, future lesion-based studies are needed to examine questions about the neural correlates of phasic autonomic functions, such as whether patients with right-lateralized degeneration will show a more sympathetic-predominant autonomic outflow deficit and how basal autonomic impairments influence phasic reactivity in the presence of cognitive and affective challenges.

Methods

Subjects. The University of California, San Francisco (UCSF) Committee on Human Research approved the study. Participants or their surrogates provided informed consent before participation. Participant medications were reviewed, and candidate control subjects were excluded if they took antihypertensive medications with known effects on the autonomic nervous system (beta-blockers, calcium channel blockers, anticholinergics, etc.).

Controls. Nineteen healthy controls (HCs) (13 females; ages 43–73 y) were recruited from the San Francisco community through advertisements as described (75). Five of 19 were unaffected family members (not carrying disease-causing genetic mutation) of patients with bvFTD. Controls were required to have a Clinical Dementia Rating (CDR) scale total score of 0, a Mini-Mental State Examination (MMSE) score of 28 or higher, no significant history of neuropsychiatric disease or structural lesion on MRI, and a consensus diagnosis of cognitively normal within 90 d of their MRI scan (Table 1 and *SI Appendix*, Table S3).

Patients. Twenty patients with bvFTD (6 female; ages 44–67 y), recruited through the UCSF Memory and Aging Center, had received a research diagnosis of bvFTD based on published criteria and had no significant history of other neurological disease (76). Patients underwent a thorough clinical evaluation, including a history, general neurological examination by a staff behavioral neurologist, CDR, MMSE, and a bedside neuropsychological screen. Patients underwent structural and functional MRI within 90 d of clinical evaluation. Three patients were taking donepezil, and their autonomic data were excluded from the main analysis (Table 1). The AD group consisted of eight patients (four female; ages 46–69 y) who underwent clinical evaluation and MRI examinations in a similar procedure as the bvFTD group, as described above. Due to the small AD sample size and the prevalence of confounding medications (donepezil) (*SI Appendix*, Table S3), the AD group was included only in supplementary analyses in which medication effects were accounted for as a binary regressor (donepezil on/off) (*SI Appendix*, Table S4). The original dataset included eight additional subjects (six patients with bvFTD, one patient with AD, and one control) who were excluded due to the poor quality of pulse oximetry recordings (see *Physiological Signal Acquisition*).

Table 1 includes three left-handed subjects (two healthy controls and one patient with bvFTD) because analyses here involved only behavioral and physiological measures of the body, where we did not expect (and did not find) left-handedness to have any impact. These left-handed participants were excluded from neuroimaging analyses.

Neuropsychological and Emotional Function Assessment. Patients were evaluated with a comprehensive neuropsychological assessment within 90 d of scanning (75, 77) (*SI Appendix*, Table S3). Guided by previous reports regarding the relationship between cardiac vagal tone and positive emotion in healthy subjects (30, 31, 44), we selected two measures that reflect positive personality traits for correlation analyses in patients with bvFTD—the personality construct "agreeableness" and personality facet "positive emotion" from the Neuroticism-Extraversion-Openness Personality Inventory-3 (NEO-PI-3) (32). First-degree relatives were asked to fill out the NEO-PI-3 questionnaire to assess the patients' current level of agreeableness, positive emotion, and other personality traits, following previous approaches to this patient group (33). Agreeableness and warmth, aspects of personality that promote social bonds and foster meaningful relationships, decline in bvFTD (33). First-degree relatives also completed the Neuropsychiatric Inventory (NPI), which captures common behavioral symptoms in dementia, including apathy and disinhibition (78), core symptoms in bvFTD. Language screening included the abbreviated Boston Naming Test (BNT) (15 items) (79), Peabody Picture Vocabulary Test (PPVT) (80), and semantic (number of animals per 1 min) and phonemic (number of D words per 1 min) word generation. Forward and backward digit span assessed executive functioning.

Partial Pearson correlation was used to analyze the correlation between personality traits and cardiac vagal tone, controlling for age, gender, and body mass index (BMI) (calculated as bodyweight in kilograms divided by height in meters squared). Because obesity can result in alterations in cardiac structure and autonomic function (81), BMI was included as a covariate to control for the effects of obesity on cardiac activity.

Physiological Signal Acquisition. ECG and pulse signals were recorded using the Siemens Physiological Monitoring Unit integrated with the Trio scanner. During scanning, heart rate was monitored using dermal ECG electrodes placed over the chest (400-Hz sampling rate) that recorded the changes in electrical signal across the heart during each beat. Pulse oximetry and heart rate were recorded using a photoplethysmograph with an infrared emitter placed under the pad of the left index finger (50-Hz sampling). Electrodermal activity was recorded using a Biopac MRI compatible acquisition system, with reusable TSD203 electrodes attaching to the right index and middle fingers (100-kHz sampling rate). Recording was automatically time-locked to the beginning of the first volume acquisition.

Physiological Signal Analysis. Physiological data were preprocessed using the PhLEM Toolbox (82) in the Matlab computing environment. Due to ECG signal corruption from an MRI-induced artifact, heartbeats could not be reliably identified from the ECG data. We therefore used pulse oximetry for heartbeat detection because its signals are not affected by an MR artifact. Although few studies have assessed clinical and older populations, pulse rate variability offers an accurate estimate of HRV at rest in healthy adults (73). The pulse oximetry recording was bandpass filtered (0.6–2.0 Hz; Butterworth filter) to remove gradient artifacts from the data. Then the filtered data were imported into the QRSTool software (35). Heart beats were identified using the built-in beat detection algorithms, followed by visual inspection where misidentified beats were manually corrected. The interbeat interval (IBI) series were then extracted and submitted to the CMetX software to derive cardiac metrics, including mean IBI, the natural log of the variance in the IBI time series (logHRV), an estimate of sympathetic-related variability [Toichi cardiac sympathetic index (CSI)], an estimate of parasympathetic-related variability Toichi cardiac vagal index (CVI), and respiratory sinus arrhythmia (RSA) [natural log of the high frequency (0.12–0.40 Hz) variance of IBI time series), and others (35). The Toichi indices (CSI and CVI) were calculated following previous methods (83). Briefly, each IBI (IBIn) was plotted against the subsequent IBI (IBIn+1) to create a Lorenz plot, where the length of the transverse axis (T) predominantly reflects parasympathetic system influence, and the length of the longitudinal axis (L) reflects both sympathetic and parasympathetic influences. The measures derived from this plot are called cardiovagal index (CVI) [Log10 ($L \times T$)] and cardiosympathetic index (CSI) (L/T). In addition, continuous HRV metrics were derived for imaging analysis, as described in *BOLD-HRV instantaneous correlation analysis*. Electrodermal activity was analyzed using the Ledalab Matlab toolbox to derive skin conductance level (SCL) and skin

conductance responses (84). Electrodermal data were discarded for one control subject due to poor recording quality.

In healthy controls, cardiac vagal tone was lower and SCL was higher in the eyes-open vs. the eyes-closed condition (*SI Appendix*, Fig. S5) ($P < 0.05$, paired t test), suggesting that these indices captured the increased alertness associated with the eyes-open condition [Barry et al. (85); Hori et al. (86)] and provide valid and sensitive measures of physiological states. Data from the eyes-open session were not analyzed further because many patients with bvFTD failed to maintain eye opening throughout the session.

Image Preprocessing and Analysis. Details regarding acquisition and preprocessing of structural and functional images are provided in *SI Appendix, Supplementary Experimental Procedures*.

BOLD-HRV instantaneous correlation analysis. Continuous HRV was calculated as the SD of IBIs within a sliding window centered on the middle of each TR. Because HRV is normally estimated using a long recording session, we used the overall CVI calculated from the entire 8-min recording as the gold standard to determine the proper length of the sliding window for deriving continuous HRV. Continuous HRV was derived with sliding windows of 2, 4, 6 ... 30 s with an acquisition interval of 2 s (the length of one TR) for each subject. With longer sliding windows, the correlation between the mean of continuous HRV and the overall HRV across all subjects increased as expected, but a sliding window of 18 s was selected because it achieved a high correlation (Pearson r of 0.976) with overall HRV while remaining short enough to provide reasonable temporal resolution. Continuous HRV was then used as a covariate of interest in a whole-brain linear regression analysis that included white matter, cerebrospinal fluid (CSF), and nonbrain (voxels that are not gray matter, white matter, or CSF) time series and six motion parameters as nuisance regressors. This procedure generated a statistical parametric map from each scan session, where each voxel was scored based on its BOLD signal correlation with the continuous HRV across the 8-min scan. Each subject's map was then entered into second-level, random-effects analyses to generate group-level connectivity maps and a two-sample t test to identify between-group differences in brain–heart coupling.

Seed-based ROI analyses. For each subject, voxel-wise intrinsic connectivity maps were derived using two seeds: the right and left FI. The right FI seed was a 4-mm spherical region-of-interest (ROI) centered at (40, 14, −12) (38). The left FI seed was the mirror image of the right FI seed, a 4-mm spherical ROI at (−40, 14, −12). FI seeds were chosen over ACC seeds due to the proximity of the ACC to the midline, which can undermine inferences regarding functional lateralization. Right and left FI-seeded intrinsic connectivity network (ICN) maps were derived separately, following previous methods [Seeley et al., 2009 (29)] (*SI Appendix, Supplementary Experimental Procedures*).

Whole brain voxel-wise degree centrality. To examine intrinsic functional connectivity without potential bias due to a priori seed selection, we computed the weighted degree centrality based on whole-brain voxel-wise connectivity (87). We first generated a group gray matter mask, covering all cortical and subcortical gray matter voxels present across all subjects in the functional imaging analyses. Then, we constructed a voxel-wise functional connectivity network for each subject, where functional connections, defined as edges, between two voxels in this map were estimated based on the Pearson's correlation coefficients between their BOLD signals. A series of thresholds ($r_{th} = 0.1, 0.3, 0.5, 0.7$) were applied to determine the presence of connections between voxels. To generate weighted adjacency matrices, each suprathreshold edge retained its correlation coefficient as its edge weight whereas subthreshold edges were assigned values of 0. Finally, voxel-wise weighted degree maps were generated by computing the weighted degree centrality of each voxel: i.e., the sum of edge weights between it and each other voxel in the group gray matter map. Because the final results generated by using different thresholds were qualitatively similar, we present only the results with $r_{threshold} = 0.5$ in the main text.

Correlational analyses between functional connectivity and cardiac vagal tone. Correlation analyses were performed using second-level analyses implemented in SPM8, following previous procedures (17, 88). Seed-based connectivity and weighted degree maps from HC and bvFTD were entered into one-sample tests. CVI or logHRV was used as the regressor of interest, and age, gender, root mean square (motion), and diagnostic groups were included as nuisance covariates. Using CVI or logHRV as the regressor of interest generated highly similar findings so, for simplicity, we reported only CVI results in the main text.

Because most clusters identified in these correlation analyses were in the left hemisphere, we performed further statistical tests of whether voxels in the left hemisphere have significantly greater correlation with CVI than the voxels in the right hemisphere. We restricted our analyses to voxels that show some correlation with CVI (loosely thresholded at $P < 0.01$, uncorrected, for height), either in the left or right hemisphere. We compared the correlation coefficients between each voxel and its mirror image in the other hemisphere using Steiger's test (89). Voxels are shown in the left hemisphere if their correlations with CVI are significantly stronger on the left than the right. Voxels are shown in the right hemisphere if their correlations with CVI are significantly stronger on the right than the left (Fig. 3*D*) ($P < 0.05$).

Statistical thresholding for whole-brain functional image analyses. Whole-brain analyses were thresholded using a joint probability distribution method to correct for multiple comparisons (90). In HC, group-level connectivity maps were generated with a threshold of $P < 0.001$ or 0.005 for height and FDR-corrected $P < 0.05$ for cluster extent (Fig. 2*A*). A generous threshold ($P < 0.01$ for height and FDR-corrected $P < 0.05$ for cluster extent) was applied to the HC result to create the explicit mask used in the two-sample t test on HRV-brain coupling maps. Group differences in HRV-brain coupling maps were evaluated at a threshold of $P < 0.01$ for height and $P < 0.05$ for extent (Fig. 2*B*). Correlation connectivity maps were generated with a threshold of $P < 0.001$ or 0.005 for height and FDR-corrected $P < 0.05$ for cluster extent (Fig. 3). To further examine whether and how observed group differences and correlations in functional maps were related to gray matter atrophy, analyses were reassessed with voxel-wise gray matter intensity maps as covariates, using the Biological Parametric Mapping (BPM) toolbox (91). All reported functional clusters remained significant after atrophy correction.

Correlation analysis of structural lateralization and cardiac vagal tone. Lateralization indices were generated from preprocessed structural images to quantify the differential atrophy between the left and right sides in patients with bvFTD (see *SI Appendix* for details). A salience network mask generated from previous studies was used to focus the analysis on core regions of injury in bvFTD (29, 39). To avoid bias introduced by asymmetries in the shape of the mask, the mask was rendered symmetric by merging the original mask with its left–right mirror image. The two halves of the resultant mask, divided by the midline, were used to calculate the average gray matter voxel intensity on the left side (V_L) and on the right side (V_R). The left-over-right lateralization index is calculated by the following equation: $(V_L - V_R)/(V_L + V_R)$. Thus, higher scores indicate more severe atrophy on the right than left and lower scores indicate more severe atrophy on the left than right. Partial correlation between the lateralization index and CVI was computed, controlling for age and gender. We further performed a voxel-wise correlation analysis between structural lateralization and cardiac vagal tone. The left-over-right lateralization index was calculated between each voxel in the salience network mask described above. The resultant lateralization index map was then subjected to a correlation analysis with CVI as the regressor of interest and age and gender as nuisance covariates.

ACKNOWLEDGMENTS. We thank our patients and their families for their invaluable contributions to neurodegeneration research and Siemens for the use of their Advanced fMRI WIP (work in progress) sequence, which allows physiology data to be recorded time-locked to the fMRI acquisition. This work was supported by NIA Grants K08 AG027086 (to W.W.S.), P50 AG023501 (to B.L.M. and W.W.S.), and P01 AG19724 (to B.L.M. and W.W.S.); the John Douglas French Foundation (W.W.S.); and the Larry L. Hillblom Foundation (W.W.S.).

1. Damasio A, Carvalho GB (2013) The nature of feelings: Evolutionary and neurobiological origins. *Nat Rev Neurosci* 14(2):143–152.
2. Critchley HD, Harrison NA (2013) Visceral influences on brain and behavior. *Neuron* 77(4):624–638.
3. Craig AD (2009) How do you feel–now? The anterior insula and human awareness. *Nat Rev Neurosci* 10(1):59–70.
4. Critchley HD (2005) Neural mechanisms of autonomic, affective, and cognitive integration. *J Comp Neurol* 493(1):154–166.
5. James W (1890) *The Principles of Psychology* (Henry Holt and Company, New York).
6. Damasio AR (1996) The somatic marker hypothesis and the possible functions of the prefrontal cortex. *Philos Trans R Soc Lond B Biol Sci* 351(1346):1413–1420.
7. Levenson RW (2003) Blood, sweat, and fears: The autonomic architecture of emotion. *Ann N Y Acad Sci* 1000(1):348–366.
8. Saper CB (2002) The central autonomic nervous system: Conscious visceral perception and autonomic pattern generation. *Annu Rev Neurosci* 25:433–469.
9. Harrison NA, Cooper E, Voon V, Miles K, Critchley HD (2013) Central autonomic network mediates cardiovascular responses to acute inflammation: Relevance to increased cardiovascular risk in depression? *Brain Behav Immun* 31:189–196.
10. Tokgözoglu SL, et al. (1999) Effects of stroke localization on cardiac autonomic balance and sudden death. *Stroke* 30(7):1307–1311.
11. Aziz NA, Anguelova GV, Marinus J, van Dijk JG, Roos RAC (2010) Autonomic symptoms in patients and pre-manifest mutation carriers of Huntington's disease. *Eur J Neurol* 17(8):1068–1074.
12. Passant U, Warkentin S, Gustafson L (1997) Orthostatic hypotension and low blood pressure in organic dementia: A study of prevalence and related clinical characteristics. *Int J Geriatr Psychiatry* 12(3):395–403.

13. Struhal W, et al. (2014) The phoenix from the ashes: Cardiovascular autonomic dysfunction in behavioral variant of frontotemporal dementia. *J Alzheimers Dis* 42(3):1041–1046.
14. Thayer JF, Brosschot JF (2005) Psychosomatics and psychopathology: Looking up and down from the brain. *Psychoneuroendocrinology* 30(10):1050–1058.
15. Thayer JF, Ahs F, Fredrikson M, Sollers JJ, 3rd, Wager TD (2012) A meta-analysis of heart rate variability and neuroimaging studies: Implications for heart rate variability as a marker of stress and health. *Neurosci Biobehav Rev* 36(2):747–756.
16. Seeley WW, Zhou J, Kim EJ (2012) Frontotemporal dementia: What can the behavioral variant teach us about human brain organization? *Neuroscientist* 18(4):373–385.
17. Seeley WW, et al. (2007) Dissociable intrinsic connectivity networks for salience processing and executive control. *J Neurosci* 27(9):2349–2356.
18. Craig AD (2002) How do you feel? Interoception: The sense of the physiological condition of the body. *Nat Rev Neurosci* 3(8):655–666.
19. Medford N, Critchley HD (2010) Conjoint activity of anterior insular and anterior cingulate cortex: Awareness and response. *Brain Struct Funct* 214(5-6):535–549.
20. Heimer L, Van Hoesen GW (2006) The limbic lobe and its output channels: Implications for emotional functions and adaptive behavior. *Neurosci Biobehav Rev* 30(2):126–147.
21. Craig AD (2005) Forebrain emotional asymmetry: A neuroanatomical basis? *Trends Cogn Sci* 9(12):566–571.
22. Oppenheimer SM, Kedem G, Martin WM (1996) Left-insular cortex lesions perturb cardiac autonomic tone in humans. *Clin Auton Res* 6(3):131–140.
23. Oppenheimer SM, Gelb A, Girvin JP, Hachinski VC (1992) Cardiovascular effects of human insular cortex stimulation. *Neurology* 42(9):1727–1732.
24. Thayer JF, Lane RD (2009) Claude Bernard and the heart-brain connection: Further elaboration of a model of neurovisceral integration. *Neurosci Biobehav Rev* 33(2): 81–88.
25. Colivicchi F, Bassi A, Santini M, Caltagirone C (2004) Cardiac autonomic derangement and arrhythmias in right-sided stroke with insular involvement. *Stroke* 35(9): 2094–2098.
26. Sturm VE, Ascher EA, Miller BL, Levenson RW (2008) Diminished self-conscious emotional responding in frontotemporal lobar degeneration patients. *Emotion* 8(6): 861–869.
27. Werner KH, et al. (2007) Emotional reactivity and emotion recognition in frontotemporal lobar degeneration. *Neurology* 69(2):148–155.
28. Seeley WW (2010) Anterior insula degeneration in frontotemporal dementia. *Brain Struct Funct* 214(5-6):465–475.
29. Seeley WW, Crawford RK, Zhou J, Miller BL, Greicius MD (2009) Neurodegenerative diseases target large-scale human brain networks. *Neuron* 62(1):42–52.
30. Fredrickson BL (2004) The broaden-and-build theory of positive emotions. *Philos Trans R Soc Lond B Biol Sci* 359(1449):1367–1378.
31. Oveis C, et al. (2009) Resting respiratory sinus arrhythmia is associated with tonic positive emotionality. *Emotion* 9(2):265–270.
32. Costa PT, McCrae RR (1992) Normal personality assessment in clinical practice: The NEO Personality Inventory. *Psychol Assess* 4(1):5–13.
33. Rankin KP, et al. (2004) Right and left medial orbitofrontal volumes show an opposite relationship to agreeableness in FTD. *Dement Geriatr Cogn Disord* 17(4):328–332.
34. Thayer JF, Hansen AL, Saus-Rose E, Johnsen BH (2009) Heart rate variability, prefrontal neural function, and cognitive performance: The neurovisceral integration perspective on self-regulation, adaptation, and health. *Ann Behav Med* 37(2):141–153.
35. Allen JJB, Chambers AS, Towers DN (2007) The many metrics of cardiac chronotropy: A pragmatic primer and a brief comparison of metrics. *Biol Psychol* 74(2):243–262.
36. Day GS, et al. (2013) Salience network resting-state activity: Prediction of frontotemporal dementia progression. *JAMA Neurol* 70(10):1249–1253.
37. Farb NA, et al. (2013) Abnormal network connectivity in frontotemporal dementia: Evidence for prefrontal isolation. *Cortex* 49(7):1856–1873.
38. Zhou J, et al. (2010) Divergent network connectivity changes in behavioural variant frontotemporal dementia and Alzheimer's disease. *Brain* 133(Pt 5):1352–1367.
39. Guo CC, et al. (2012) One-year test-retest reliability of intrinsic connectivity network fMRI in older adults. *Neuroimage* 61(4):1471–1483.
40. Di Martino A, et al. (2009) Relationship between cingulo-insular functional connectivity and autistic traits in neurotypical adults. *Am J Psychiatry* 166(8):891–899.
41. Stanley ML, et al. (2013) Defining nodes in complex brain networks. *Front Comput Neurosci* 7(November):169.
42. Rankin KP, Kramer JH, Miller BL (2005) Patterns of cognitive and emotional empathy in frontotemporal lobar degeneration. *Cogn Behav Neurol* 18(1):28–36.
43. Porges SW (2007) The polyvagal perspective. *Biol Psychol* 74(2):116–143.
44. Kok BE, Fredrickson BL (2010) Upward spirals of the heart: Autonomic flexibility, as indexed by vagal tone, reciprocally and prospectively predicts positive emotions and social connectedness. *Biol Psychol* 85(3):432–436.
45. Yoon B-W, Morillo CA, Cechetto DF, Hachinski V (1997) Cerebral hemispheric lateralization in cardiac autonomic control. *Arch Neurol* 54(6):741–744.
46. Wittling W (1997) Brain asymmetry and autonomic control of the heart. *Eur Psychol* 2(4):313–327.
47. Zamrini EY, et al. (1990) Unilateral cerebral inactivation produces differential left/right heart rate responses. *Neurology* 40(9):1408–1411.
48. Hilz MJ, et al. (2001) Hemispheric influence on autonomic modulation and baroreflex sensitivity. *Ann Neurol* 49(5):575–584.
49. Robinson TG, James M, Youde J, Panerai R, Potter J (1997) Cardiac baroreceptor sensitivity is impaired after acute stroke. *Stroke* 28(9):1671–1676.
50. Wittling W, Block A, Genzel S, Schweiger E (1998) Hemisphere asymmetry in parasympathetic control of the heart. *Neuropsychologia* 36(5):461–468.
51. Barron SA, Rogovski Z, Hemli J (1994) Autonomic consequences of cerebral hemisphere infarction. *Stroke* 25(1):113–116.
52. Naver HK, Blomstrand C, Wallin BG (1996) Reduced heart rate variability after right-sided stroke. *Stroke* 27(2):247–251.
53. Massetani R, et al. (1997) Alteration of cardiac function in patients with temporal lobe epilepsy: Different roles of EEG-ECG monitoring and spectral analysis of RR variability. *Epilepsia* 38(3):363–369.
54. Ahern GL, et al. (2001) Heart rate and heart rate variability changes in the intracarotid sodium amobarbital test. *Epilepsia* 42(7):912–921.
55. Cacioppo JT, et al. (2003) Just because you're imaging the brain doesn't mean you can stop using your head: A primer and set of first principles. *J Pers Soc Psychol* 85(4): 650–661.
56. Critchley HD (2009) Psychophysiology of neural, cognitive and affective integration: fMRI and autonomic indicants. *Int J Psychophysiol* 73(2):88–94.
57. Kreibig SD (2010) Autonomic nervous system activity in emotion: A review. *Biol Psychol* 84(3):394–421.
58. Grossman P, Taylor EW (2007) Toward understanding respiratory sinus arrhythmia: Relations to cardiac vagal tone, evolution and biobehavioral functions. *Biol Psychol* 74(2):263–285.
59. Moon E, Lee S-H, Kim D-H, Hwang B (2013) Comparative study of heart rate variability in patients with schizophrenia, bipolar disorder, post-traumatic stress disorder, or major depressive disorder. *Clin Psychopharmacol Neurosci* 11(3): 137–143.
60. Chalmers JA, Quintana DS, Abbott MJ-A, Kemp AH (2014) Anxiety disorders are associated with reduced heart rate variability: A meta-analysis. *Front Psychiatry* 5:80.
61. Thayer JF, Friedman BH, Borkovec TD (1996) Autonomic characteristics of generalized anxiety disorder and worry. *Biol Psychiatry* 39(4):255–266.
62. Blechert J, Michael T, Grossman P, Lajtman M, Wilhelm FH (2007) Autonomic and respiratory characteristics of posttraumatic stress disorder and panic disorder. *Psychosom Med* 69(9):935–943.
63. Gruber J, Johnson SL, Oveis C, Keltner D (2008) Risk for mania and positive emotional responding: Too much of a good thing? *Emotion* 8(1):23–33.
64. Kogan A, et al. (2014) Vagal activity is quadratically related to prosocial traits, prosocial emotions, and observer perceptions of prosociality. *J Pers Soc Psychol* 107(6): 1051–1063.
65. Rankin KP, et al. (2006) Structural anatomy of empathy in neurodegenerative disease. *Brain* 129(Pt 11):2945–2956.
66. Kim E-J, et al. (2012) Selective frontoinsular von Economo neuron and fork cell loss in early behavioral variant frontotemporal dementia. *Cereb Cortex* 22(2):251–259.
67. Woolley JD, et al. (2007) Binge eating is associated with right orbitofrontal-insular-striatal atrophy in frontotemporal dementia. *Neurology* 69(14):1424–1433.
68. Sturm VE, et al. (2013) Role of right pregenual anterior cingulate cortex in self-conscious emotional reactivity. *Soc Cogn Affect Neurosci* 8(4):468–474.
69. Sturm VE, et al. (2015) Damage to left frontal regulatory circuits produces greater positive emotional reactivity in frontotemporal dementia. *Cortex* 64:55–67.
70. Demaree HA, Everhart DE, Youngstrom EA, Harrison DW (2005) Brain lateralization of emotional processing: Historical roots and a future incorporating "dominance". *Behav Cogn Neurosci Rev* 4(1):3–20.
71. Sturm VE, Rosen HJ, Allison S, Miller BL, Levenson RW (2006) Self-conscious emotion deficits in frontotemporal lobar degeneration. *Brain* 129(Pt 9):2508–2516.
72. Joshi A, et al. (2014) Skin conductance levels may reflect emotional blunting in behavioral variant frontotemporal dementia. *J Neuropsychiatry Clin Neurosci* 26(3): 227–232.
73. Schäfer A, Vagedes J (2013) How accurate is pulse rate variability as an estimate of heart rate variability? A review on studies comparing photoplethysmographic technology with an electrocardiogram. *Int J Cardiol* 166(1):15–29.
74. Beissner F, Meissner K, Bär K-J, Napadow V (2013) The autonomic brain: An activation likelihood estimation meta-analysis for central processing of autonomic function. *J Neurosci* 33(25):10503–10511.
75. Rosen HJ, et al. (2002) Patterns of brain atrophy in frontotemporal dementia and semantic dementia. *Neurology* 58(2):198–208.
76. Neary D, et al. (1998) Frontotemporal lobar degeneration: A consensus on clinical diagnostic criteria. *Neurology* 51(6):1546–1554.
77. Rankin KP, et al. (2009) Detecting sarcasm from paralinguistic cues: Anatomic and cognitive correlates in neurodegenerative disease. *Neuroimage* 47(4):2005–2015.
78. Rosen HJ, et al. (2005) Neuroanatomical correlates of behavioural disorders in dementia. *Brain* 128(Pt 11):2612–2625.
79. Kaplan EF, Goodglass H, Weintraub S (1983) *The Boston Naming Test* (Lea & Febiger, Philadelphia).
80. Dunn LM (1970) *Expanded Manual for the Peabody Picture Vocabulary Test* (American Guidance Service, Minneapolis).
81. Alpert MA, Hashimi MW (1993) Obesity and the heart. *Am J Med Sci* 306(2):117–123.
82. Verstynen TD, Deshpande V (2011) Using pulse oximetry to account for high and low frequency physiological artifacts in the BOLD signal. *Neuroimage* 55(4): 1633–1644.
83. Toichi M, Sugiura T, Murai T, Sengoku A (1997) A new method of assessing cardiac autonomic function and its comparison with spectral analysis and coefficient of variation of R-R interval. *J Auton Nerv Syst* 62(1-2):79–84.
84. Benedek M, Kaernbach C (2010) A continuous measure of phasic electrodermal activity. *J Neurosci Methods* 190(1):80–91.
85. Barry RJ, Clarke AR, Johnstone SJ, Magee CA, Rushby JA (2007) EEG differences between eyes-closed and eyes-open resting conditions. *Clin Neurophysiol* 118(12): 2765–2773.
86. Hori K, et al. (2005) Influence of sound and light on heart rate variability. *J Hum Ergol* 34(1-2):25–34.
87. Liao X-H, et al. (2013) Functional brain hubs and their test-retest reliability: A multiband resting-state functional MRI study. *Neuroimage* 83:969–982.
88. Guo CC, et al. (2013) Anterior temporal lobe degeneration produces widespread network-driven dysfunction. *Brain* 136(Pt 10):2979–2991.

89. Steiger JH (1980) Tests for comparing elements of a correlation matrix. *Psychol Bull* 87(2):245–251.
90. Poline JB, Worsley KJ, Evans AC, Friston KJ (1997) Combining spatial extent and peak intensity to test for activations in functional imaging. *Neuroimage* 5(2):83–96.
91. Casanova R, et al. (2007) Biological parametric mapping: A statistical toolbox for multimodality brain image analysis. *Neuroimage* 34(1):137–143.
92. Menon V, Uddin LQ (2010) Saliency, switching, attention and control: A network model of insula function. *Brain Struct Funct* 214(5-6):655–667.